2020 IEEE/RSJ International Conference on Intelligent Robots and Systems (IROS)
October 25-29, 2020, Las Vegas, NV, USA (Virtual)

Ultra Low-Cost Printable Folding Robots

Saul Schaffer[1], Emily Wang[1], Nathan Cooper[1], Bo Li[3], Zeynep Temel[4], Ozan Akkus[3]
Victoria A. Webster-Wood [1,2*]

***Abstract*— Current techniques in robot design and fabrication are time consuming and costly. Robot designs are needed that facilitate low-cost fabrication techniques and reduce the design to production timeline. Here we present an axial-rotational coupled metastructure that can serve as the functional core of a low-cost 3D printed walking robot. Using an origami-inspired assembly technique, the axial-rotational coupled metastructure robot can be 3D printed flat and then folded into a final configuration. This print-then-fold approach allows for the facile integration of critical subcomponents during the printing process. The axial-rotational metastructures eliminate the need for joints and linkages by enabling locomotion through a single compliant structure. Finite element models of the axial-rotational metastructures were developed and validated against experimental deformation of 3D printed units under tensile loading. As a proof-of-concept, an ultra low-cost 3D-printed metabot was designed and fabricated using the proposed axial-rotational coupled metastructure and its walking performance was characterized. A top speed of 4.30 mm/s was achieved with an alternating stepping gait at a frequency of 0.8 Hz.**

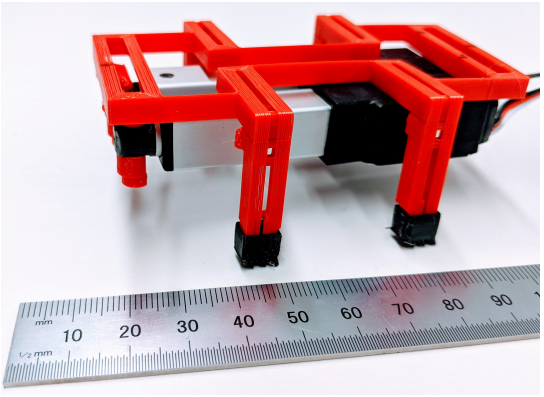

Fig. 1. metabot: 92.5 mm long, 41 mm wide and 39 mm tall. Two magnets are embedded on either side of each joint (8 in total). The mass of the entire robot (structure, actuators, magnets) is 79 g. The total cost of the robot sans the actuators is US$0.69. Total print and subcomponent embedding time was 78 minutes.

I. INTRODUCTION

The current paradigm for fabricating highly intricate mechanisms like robots requires time and capital-intensive design and iteration loops. A slew of additional infrastructure like molds, jigs, and fixtures are needed for the fabrication of current robots, thereby dramatically increasing the monetary cost and person-hours necessary to realize a new design. A number of fabrication techniques have been investigated to reduce these costs, including origami and 3D printing, which show great potential for robotic applications.

By starting from a flat sheet, fabrication of origami robots can be accomplished with a wide variety of planar fabrication techniques. Planar manufacturing methods have the advantage of being relatively fast in comparison to other techniques such as machining. One common approach called Smart Composite Microstructures (SCM) consists of stacking thin layers of functional materials. These stacks are then laser patterned and laminated [1]–[3]. SCM has enabled breakthrough work in microscale origami robotics [4], [5], and similar methods have been successfully deployed at the macroscale [6]. Though a complete review of origami robots is beyond the scope of the current paper, interested readers are encouraged to refer to Rus and Tolley [7] for a comprehensive review. Furthermore, 3D printing can further enable origami robotics by adding additional functionalities that would be difficult to achieve with traditional planar fabrication methods.

3D printing presents a facile way to overcome conventional fabrication and assembly challenges. Instead of creating separate components for later assembly, functional and intricate 3D printed structures can be strategically designed and fabricated as single parts. Many groups have made use of 4D printing, or the practice of 3D printing an object that then changes shape over time in response to some stimulus (e.g. heat, light, magnetic field) [8], [9]. The most common 3D printing modality for printed robots is Polyjet [10]–[13], in which droplets of photocurable inks are jetted onto a substrate and cured with a UV lamp in a layer-by-layer process. Polyjet 3D printing not only provides a high layer resolution of 16 μm [14], but also allows for simultaneous printing of multiple materials. This capability allows for single parts that have variable compliance [15]. A more in-depth review of 3D printing and its robotic applications has been conducted by Gul *et al.* [16].

Although previous work in origami and 3D printed robotics has led to numerous exciting robotic systems, current application of these techniques in robotics is often quite expensive. Most current origami robots rely on techniques that require costly equipment for fabrication such as Polyjet 3D printing or laser micro-machining. The machines that enable these techniques are often closed-source and cost upwards of US$300,000. In the case of Polyjet 3D printing,

*Corresponding Author: vwebster@andrew.cmu.edu
[1]Department of Mechanical Engineering, Carnegie Mellon University, Pittsburgh, PA, 15213
[2]Department of Biomedical Engineering, by courtesy, Carnegie Mellon University, Pittsburgh, PA, 15213
[3]Department of Mechanical and Aerospace Engineering, Case Western Reserve University, Cleveland, OH, 44106
[4]Robotics Institute, Carnegie Mellon University, Pittsburgh, PA, 15213

the cost of the materials and maintenance of the machine balloon this cost over the lifetime of the machine.

In contrast, Fused Deposition Modeling (FDM) 3D printing offers inexpensive alternatives with consumer grade machines. FDM 3D printers provide a more economically accessible and easily configurable platform for researchers and educators to develop robotic systems due to their low cost and tendency to be open source. Despite being inexpensive, these machines still maintain a relatively high layer resolution with many able to achieve feature sizes of 300 μm [17]. With FDM 3D printers, as with most 3D printing methods, morphological complexity is not penalized in terms of cost and fabrication time as severely as it is with traditional fabrication methods. As such, novel morphological structures such as mechanical metastructures can be fabricated with ease. These metastructures enable functional behaviors to be 'programmed' into the mechanics of the part.

An under-explored class of mechanical metastructures with axial-rotational coupling has the potential to reduce time and capital costs incurred in robot fabrication. These Axial-Rotational Coupled (AxRoC) structures have the potential to greatly expand the space in which robotic systems can be designed. Preliminary results suggest that coupled AxRoC metastructures can enable functional gait for tremendously low cost. Because these mechanisms are continuous and compliant, they do not experience any backlash or friction. Leveraging AxRoC metastructures, the authors demonstrate preliminary results that functional gait can be mechanically programmed in the robot's structure.

This work seeks to fill two key gaps in the existing literature. Firstly, the cost to fabricate 3D printed origami robots – though not explicitly reported in the literature – is estimated to be on the order of tens of thousands of dollars due to the cost of Polyjet 3D printers, the machines most often employed in previous work [7]. In contrast, our proof-of-concept robot (Figure 1) has material costs on the order of cents, with a vast majority of the equipment cost dedicated to the overhead for an FDM 3D printer (US$750) and actuators (US$70 each). Additionally, having the robot structure 3D printed allows for other synergies to emerge, such as embedding functional components like actuators directly into the core structure of the robot. Such embedding removes the need for fasteners. Lastly, the existing literature lacks instances of axial-rotational coupled metastructures for robotic applications [18], a gap filled by our work.

In this paper, we will present the design, modeling and characterization of an ultra low-cost AxRoC metastructure robot. A finite element analysis was developed to aid future robot design and validated through mechanical characterization of 3D printed realizations of a simple AxRoC structure. Furthermore, we demonstrate two additional functionalities: facile folding and embedding functional components with zero fasteners. These functionalities were manifest in a prototype walking robot with AxRoC-enabled gaits.

II. METHODS

The proposed AxRoC-based functional core consists of a biaxially-symmetric frame in which four AxRoC units are positioned as shown in Figure 2. When the metastructure is subjected to axial tensile load, each AxRoC unit rotates in relation to the amount of force applied to the frame. Within each AxRoC structure, there are two thin, flexible beams as well as a rigid central hub. When load is applied to the frame segments most distal to the transverse axis, the thin beams are subjected to a bending load and begin to bow. As a result, the central hub rotates by an angle θ. It is precisely this angle θ that the authors are interested in investigating, as strategically attaching footed segments to the rotating hubs can enable a reciprocating curved sweeping gait instead of a simpler reciprocating linear gait.

The length L of the central hub is critical to how much the hub will rotate as its length serves as the moment arm that leads to rotation under the action of a tensile force to the frame. To investigate the relationship between length L and rotation θ, the value of L was varied for a given AxRoC structure and the output θ was measured during loading both in simulation and experimentally. Additionally, a prototype AxRoC metastructure robot was built. The prototype robot featured a functional core within the parameter space explored computationally and featured the addition of legs that extended out distally from each AxRoC hub. This robot prototype was printed with actuators embedded during the print process and living hinges that allow legs to be printed flat – and therefore faster – that can then fold. To facilitate facile folding, one magnet was embedded in either end of the living hinge during printing. This arrangement enabled folding from the printed configuration to the final configuration to be initiated with a simple bend of the legs.

A. Finite Element Analysis

Finite element analysis was conducted to investigate the effect of varying the critical length parameter L on the rotational response of the AxRoC hub. Simulations were conducted using the finite element analysis software ANSYS. Linear tetrahedral elements were employed at the discretion of the software. Mesh convergence was considered achieved when the variation of the von Mises stress was within 10%. To match our experiments, we assigned Polylactic

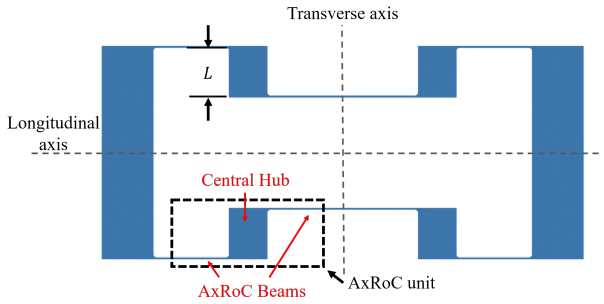

Fig. 2. Schematic for AxRoC metastructure functional core.

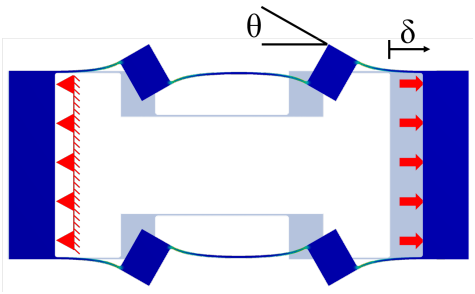

Fig. 3. Loading boundary conditions for ANSYS simulation and experimental testing. Left-most inner surface assigned a fixed boundary condition and right-most inner surface given a steadily increasing distributed load.

Component	Print time	Weight	Cost (USD)
AxRoC functional core	65 mins	9.2 g	$0.18
Compliant feet (x4)	13 mins	0.93 g	$0.03
Embedded magnets (x8)	—	0.58 g	$0.48
Linear actuators (x2)	—	34 g	$140

TABLE I

RELEVANT VALUES FOR EACH COMPONENT INCLUDED IN THE PROTOTYPE AXROC METASTRUCTURE ROBOT. THE MULTIPLIERS INDICATE THE NUMBER OF EACH UNIT INCLUDED IN THE TOTAL COST.

Acid (PLA) to be our material for simulation. The default PLA material model found in ANSYS Workbench 2019R2 was used with a Young's modulus of 3.0 GPa based on the findings of Letcher and Waytashek [19]. An isotropic linear elastic material model was used with a Poisson's ratio of 0.39. It should be noted that 3D printed plastics have a number of critical mechanical properties such as tensile strength, ultimate strength, and Young's modulus that vary widely depending on the printing parameters used [19]–[21]. For our analysis, we chose to use a value for the Young's modulus that was determined in loading conditions similar to those experienced by the AxRoC beams, namely bending.

The boundary conditions for the simulation are shown in Figure 3. A fixed boundary condition was applied to the interior surface of one edge of the frame and the opposing surface, indicated by red arrows, was given a load that increased from 1 N to 20 N along the longitudinal axis over the course of 20 seconds. The time steps were constrained to no more than 0.1 seconds and no less than two milliseconds. The mesh physics preference was set to Mechanical and Large Deflections were enabled.

Due to the 3D printing process, the geometry of resulting parts does not exactly match the geometry used for slicing. As a consequence, the model used in the simulation was updated to more closely match the final printed geometry. In FDM 3D printing, the thickness of a 3D printed part is limited to a multiple of the width of the print bead, which corresponds to the nozzle diameter of the extruder. As such, a designed geometry of 0.5 mm thick AxRoC beams resulted in an average printed thickness of 0.75 mm. A similar modification was necessary for the height of the simulated model, as the printed part was 5.1 mm in height instead of the designed 5.0 mm. Only the height of the structure and the width of the thin beams were affected; the rest of the model's parameters were unaffected by the printing discrepancies. The outputs of the model were the displacement of the surface most distal from the fixed boundary condition and change in angle of an edge of an AxRoC hub. The angle measurement was achieved by placing a Remote Point line along the edge of one of the AxRoC hubs and tracking its rotation about the axis orthogonal to the longitudinal and transverse axes using a Flexible Rotation Probe. Because of the symmetry of the system, the absolute magnitude of the rotation angle is the same for all AxRoC hubs within a given functional core.

B. Fabrication

AxRoC metastructures and robots were fabricated using a low-cost open source and commercially available 3D printer (Prusa i3 MK3S, Prusa Research) using PLA plastic filament (PLA 1.75 mm, Hatchbox 3D). During printing, subcomponents were manually embedded in the structure during a pause introduced as part of normal slicing. Embedded components included 6 mm by 3 mm magnets to facilitate folding to the final configuration (FINDMAG, Amazon) and two L12-R micro linear servos for actuation (Actuonix L12-30-50-6-R). These actuators served as the source of the reciprocating linear motion that drives the metabot's locomotion. Peripheral components including an Arduino Nano for control and a 7.4 V lithium polymer battery were not embedded during the printing process. Frictionally-biased press-on feet were 3D printed separately using a flexible thermoplastic polyurethane (1.75 mm CheetahFlex TPU) on the same printer. Total print time, including the time to embed the magnets and actuators during the print, is 65 minutes for the main structure and 13 mins for the swappable feet. Weight, cost, and print time for each component can be found in Table II-B.

To allow the robot to be printed flat, yet take on a 3D final configuration, thin, single layers of PLA (300 μm) are used to attach the legs to the body as seen in Figure 4 (inset A.2). The length of these thin flexures is twice the layer height of the print (2×0.2 mm) plus the height of the segment it was designed to fold over. Magnets are fitted into opposing appendages to fix legs semi-permanently into position following folding. Only a single fold is needed to affix a leg in its final configuration. The printed and final configurations are shown in Figure 4 (A and B, respectively).

To achieve the desired folding, appropriate slice settings were determined empirically (PrusaSlicer v2.1.0). Global print parameters were set at 0.2 mm layer height with no (0%) infill and 4 perimeters. These settings were chosen to accelerate print time, as well as to eliminate the mechanically anisotropic effects of infill. By slicing the print in this way, the deposition of all print beads run as continuous lines, as seen in Figure 5. In addition to the global parameters, the first layer of the print was modified to have eight perimeters.

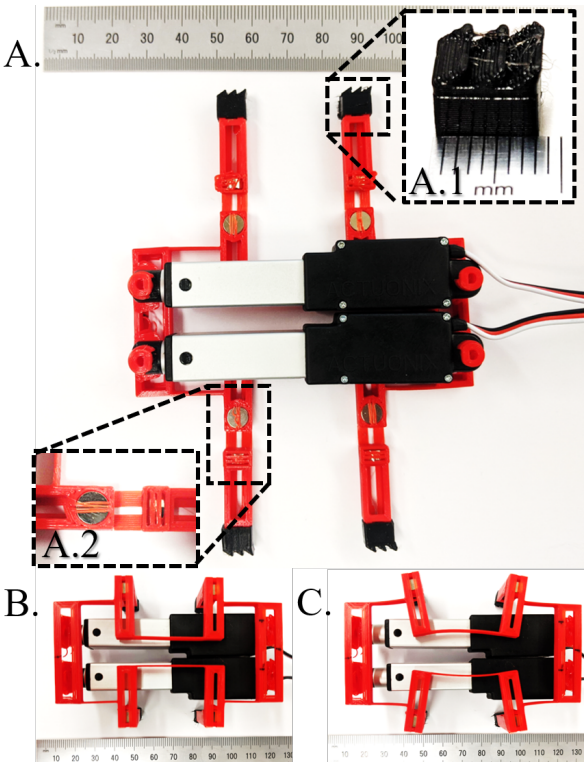

Fig. 4. A) Unfolded AxRoC metastructure prototype. Magnets (inset A.2), to facilitate folding, and actuators were embedded into the structure during the print process and thus do not require any fasteners. Folding of all four legs from the print configuration to the final configuration takes approximately three seconds and is done by folding the printed living hinges (inset A.2) by hand. Friction-biased 3D printed feet (inset A.1) are pressed onto the legs during final assembly. B) Top view of folded prototype robot in closed phase of gait cycle and C) open phase of gait cycle.

This choice was made to increase the area of the first layer to combat print delamination from the print bed.

C. Mechanical Characterization

To quantify the mechanical response to load of the 3D printed metastructures and to validate the ANSYS simulation, samples were loaded in a universal testing machine (MTS Criteron Model 42) at 10 mm/min and force was measured with a 50 N load cell. Custom 3D printed passive fixtures were fabricated to secure the samples. During this loading, a camera recorded the deformation of the AxRoC units. The free video analysis software Tracker [22] was used to extract the change in angle of AxRoC hubs in response to loading. Two tracking points were assigned to the edge of each AxRoC hub for a total of eight points tracked per trial. From the change in x-y pixel coordinates for the two points tracked on each hub, the rotation angle was calculated as:

$$\theta = atan2(||\vec{V}_1 \times \vec{V}_2||, \vec{V}_1 \cdot \vec{V}_2) \times \frac{180^\circ}{\pi}$$

Where $\vec{V}_1$ is the vector defined by the initial position on the AxRoC hub and $\vec{V}_2$ is the vector defined by two points on the AxRoC hub as it rotates. Using the atan2 function ensures that the values returned are all in the same quadrant.

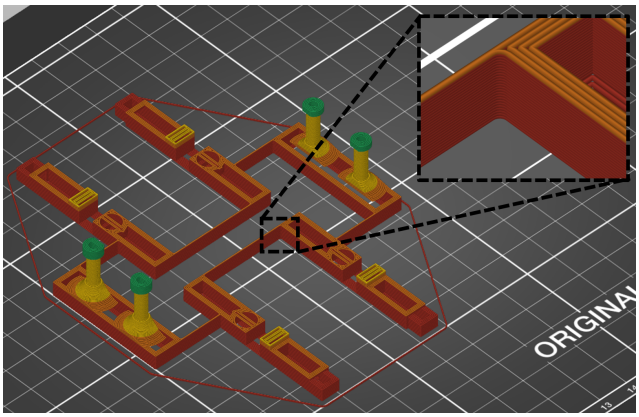

Fig. 5. Render of 3D print toolpath generated by the slicer. Each color change indicates a print height at which a subcomponent is inserted mid-print. The red-orange and orange-yellow interfaces indicate the layers for the insertion of magnets while the yellow-green transition indicates the pause for embedding the two linear actuators. The inset showcases that the AxRoC beams are formed from two print beads printed next to each other in a continuous linear deposition without any cross hatching. This is to eliminate any anisotropic effects from infill in the beams.

For clarity, this angle is shown in Figure 3. Angle data from video analysis was combined with force data from the MTS to determine the force versus angle relationship for different values of the L length parameter.

D. Robot Prototype

To demonstrate the efficacy of AxRoC metastructures to produce functional gaits, a prototype robot was constructed and evaluated as shown in Figure 4. The prototype metastructure robot or metabot was 3D printed as two pieces: *i)* a core body structure with embedded functional components and *ii)* compliant feet printed in a separate, more flexible TPU material as shown in Figure 4 (inset A.1). The anisotropy of the feet results in frictional anisotropy when in contact with the ground, allowing the feet to slip when pushed in one direction and stick when pushed in the opposite direction. This anisotropic friction allows the robot to walk.

Two robot gaits were investigated. In both gaits, the actuation extension distance and frequency were set to 5 mm and 0.8 Hz, respectively. First, the robot used a gait that consisted of a closed phase and an open phase as shown in Figure 4 (B-C). In the closed phase, both actuators were fully retracted. In the open phase, both actuators were set to extend 5 mm. By alternating between these phases, locomotion was achieved. Six trials with this gait were conducted. In three trials, the feet were aligned with the wedges pointed towards the extendable side of the actuators. In the other three, the feet were rotated 180°. In all six trials, the wedges were pointing in the opposite direction of locomotion. In one trial, the robot was observed to become stuck and cease forward progress. This trial was excluded from further analysis. The second gait tested used a stepping pattern in which the two actuators alternated between the open and closed positions out of phase with each other. Both gaits result in sweeping motions of the feet by virtue of the 'programmed' mechanics

of the structure.

The robot was tested carrying a payload that weighed 88 g consisting of a breadboard, wires, Arduino Nano, and battery. The robot itself consisted of two actuators embedded within a core AxRoC structure along with eight magnets for a total weight of 79 g. The robot's locomotion was recorded with a camera positioned above the robot. As with the mechanical tests, a fixed point was tracked through every frame of the walking trials using Tracker [22] software. The x-y position and displacement over time were analysed in MATLAB.

III. RESULTS AND DISCUSSION

A. Validation of Model Performance

The ANSYS simulation predicts θ-Force trends observed in the experimental characterization of the AxRoC metastructure. Values of the L length parameter ranging from 1.5 mm to 20 mm in 0.5 mm increments were simulated. A subset of that range (L = 5 mm, 10 mm, 15 mm) were 3D printed and experimentally characterized. Figure 6 showcases the linear relationship between L and the maximum rotation angle θ, which agrees with our intuition. The authors noticed that there was a bifurcation in experimental θ-Force data with AxRoC units on one side of the longitudinal axis exhibiting similar rotation angles while contralateral AxRoC units had slight discrepancies in rotation angle (data not shown). This is likely due to slightly unequal loading of the AxRoC functional core during the MTS test caused by subtle surface roughness at the interface of the 3D printed fixtures and the metastructure cores. Additionally, subtle plastic deformation was observed after AxRoC tensile tests, leading to experimental and simulation results deviating slightly for larger L values. Even with these minor discrepancies, the model presents a useful tool for metabot design.

Equipped with this functional numerical model, future applications of this work include: *i)* applying the model to other 3D printed materials such as ABS or PETG, *ii)* optimizing the performance of the metastructure by varying its complexity through numerical simulations, and *iii)* identifying the potential failure mechanisms of the metastructure.

B. Prototype Walking AxRoC Metastructure Robot

The prototype AxRoC metastructure robot was able to achieve forward locomotion with two 0.8 Hz gaits, a simple bilateral expansion and contraction as well as a stepping gait (Figure 7). As the frictionally-biased swappable feet can be easily exchanged, the performance of the robot with feet oriented such that the wedges slant towards the extendable side of the actuators (Foot Direction 1), and with the feet rotated 180° (Foot Direction 2, see Figure 4) was investigated. In both cases, the positive forward locomotion direction of the robot is defined by the direction of the feet. All robot trials shown in Figure 7 started with the robot aligned along the x-axis. Foot Direction 2 resulted in noticeable slipping and turning during locomotion as compared to Foot Direction 1. In the Foot Direction 1 configuration, the rear feet of the robot were supporting more weight due to the weight distribution of the actuators and as such were less susceptible

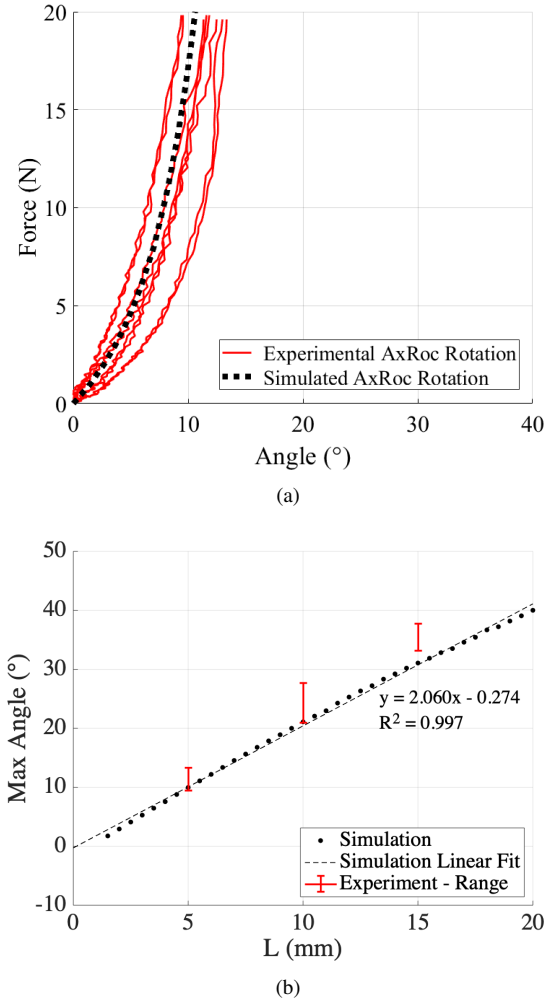

Fig. 6. Comparisons of experimental and simulated AxRoC performance. *a)* Plot of θ-Force relationships for representative AxRoC metastructure core with L = 5 mm. *b)* Plot of maximum rotational deflection as a function of L, showing agreement between simulated and experimental results.

to slipping backwards while the robot went from the closed phase to the open phase of gait. When the direction of the feet, and therefore the direction of robot was flipped, the front feet now supported more weight than the back feet which resulted in more slipping of the back feet. For the tested gaits, the stepping gait resulted in the most robust forward locomotion.

IV. CONCLUSION

Demonstrated in this work is a method for realizing ultra low-cost, foldable, mechanical metastructure robots. The response and performance of the structure under tensile loads can be tuned by varying key internal geometries. We presented a finite element model that captures the relevant behaviors of the metastructure and validated the model experimentally. A prototype metastructure robot based on the AxRoC metastructure was able to achieve forward locomotion in two separate gaits by leveraging the mechanical programming of the metastructure. Due to the low cost of

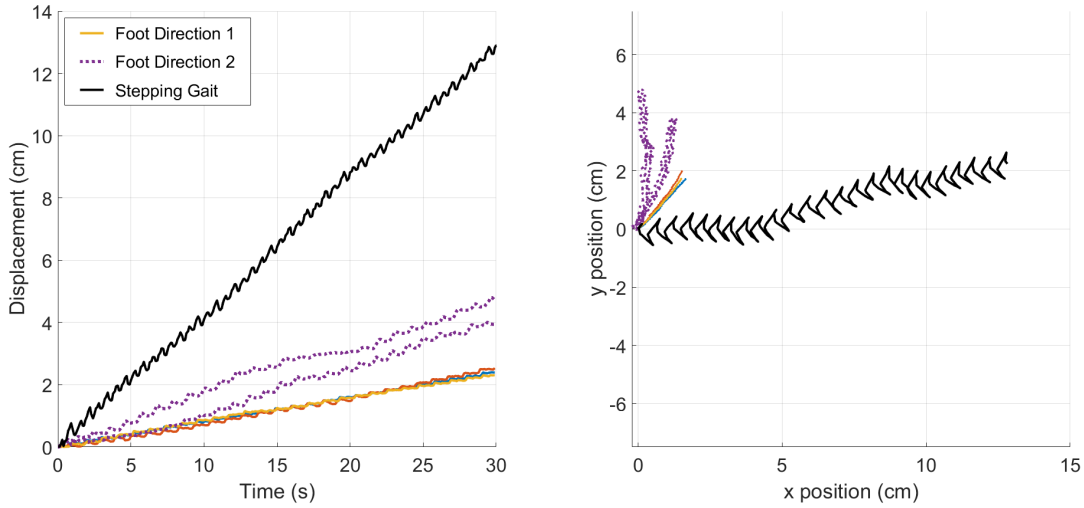

(a) (b)

Fig. 7. a) Total displacement of the leading edge of the robot using the bilateral expansion/contraction gait with feet slanted towards the extendable side of the actuator (solid colored lines), with feet rotated 180° (dotted lines) and using an alternating stepping gait (solid black line). b) X-Y traces of the motion of the leading edge of the robot. Only the stepping gait produced substantial forward locomotion with minimal rotation, at a rate of 4.30 mm/s.

fabrication for such AxRoC metabots, and the simplicity of fabrication, such devices have great potential in engineering education and outreach, or in applications where low-cost disposable robots are needed. The developed model can provide a foundation for the future development of generative design tools to increase AxRoC metabot functionality by programming additional behaviors into the flexible structure.

V. ACKNOWLEDGEMENTS

This work was supported by the Carnegie Mellon University Department of Mechanical Engineering. The authors would like to thank Wenhuan Sun for his instruction on the use of the MTS Criteron Electromechanical Test System.

REFERENCES

[1] R. J. Wood, S. Avadhanula, R. Sahai, E. Steltz, and R. S. Fearing, "Microrobot design using fiber reinforced composites," *Journal of Mechanical Design, Transactions of the ASME*, vol. 130, no. 5, 2008.

[2] K. L. Hoffman and R. J. Wood, "Myriapod-like ambulation of a segmented microrobot," *Autonomous Robots*, vol. 31, no. 1, pp. 103–114, 7 2011.

[3] H. McClintock, F. Z. Temel, N. Doshi, J.-s. Koh, and R. J. Wood, "The milliDelta: A high-bandwidth, high-precision, millimeter-scale Delta robot," *Science Robotics*, vol. 3, no. 14, pp. 1–9, 1 2018.

[4] R. Wood, R. Nagpal, and G.-Y. Wei, "Flight of the robobees," Tech. Rep., 2013.

[5] N. Jafferis, F. Helbling, M. Karpelson, and R. J. Wood, "Untethered flight of an insect-sized flapping-wing microscale aerial vehicle," *Nature*, vol. 570, pp. 491–495, 2019.

[6] S. Felton, M. Tolley, E. Demaine, D. Rus, and R. Wood, "A method for building self-folding machines," *Science*, vol. 345, no. 6197, pp. 644–646, 2014.

[7] D. Rus and M. T. Tolley, "Design, fabrication and control of origami robots," *Nature Reviews Materials*, 2018.

[8] H. Ding, X. Zhang, Y. Liu, and S. Ramakrishna, "Review of mechanisms and deformation behaviors in 4D printing."

[9] Z. X. Khoo, J. E. M. Teoh, Y. Liu, C. K. Chua, S. Yang, J. An, K. F. Leong, and W. Y. Yeong, "3D printing of smart materials: A review on recent progresses in 4D printing," *Virtual and Physical Prototyping*, vol. 10, no. 3, pp. 103–122, 2015.

[10] V. Megaro, S. Coros, J. Zehnder, M. Bächer, M. Gross, and B. Thomaszewski, "A computational design tool for compliant mechanisms," *ACM Transactions on Graphics*, vol. 36, no. 4, pp. 1–12, 2017.

[11] J. Neubert and H. Lipson, "Soldercubes: a self-soldering self-reconfiguring modular robot system," *Autonomous Robots*, vol. 40, no. 1, pp. 139–158, 1 2016.

[12] N. Bartlett, M. Tolley, J. Overvelde, J. Weaver, B. Mosadegh, K. Bertoldi, G. Whitesides, and R. J. Wood, "A 3D-printed, functionally graded soft robot powered by combustion," *Science*, vol. 349, no. 6244, pp. 161–165, 2015.

[13] C. H. Belke and J. Paik, "Mori: A Modular Origami Robot," *IEEE/ASME Transactions on Mechatronics*, vol. 22, no. 5, pp. 2153–2164, 10 2017.

[14] Stratasys, "Objet500 Connex3 Datasheet," Tech. Rep., 2016. [Online]. Available: https://www.stratasys.com/3d-printers/objet-350-500-connex3

[15] J. Y. Lee, W. B. Kim, W. Y. Choi, and K. J. Cho, "Soft Robotic Blocks: Introducing SoBL, a Fast-Build Modularized Design Block," *IEEE Robotics and Automation Magazine*, vol. 23, no. 3, pp. 30–41, 2016.

[16] J. Z. Gul, M. Sajid, M. M. Rehman, G. U. Siddiqui, I. Shah, K.-H. Kim, J.-W. Lee, and K. H. Choi, "3D printing for soft robotics - a review," *Science and technology of advanced materials*, vol. 19, no. 1, pp. 243–262, 2018.

[17] V. Romanov, R. Samuel, M. Chaharlang, A. R. Jafek, A. Frost, and B. K. Gale, "FDM 3D Printing of High-Pressure, Heat-Resistant, Transparent Microfluidic Devices," 2018.

[18] R. Bomer and P. Smagorinsky, *Handbook of Compliant Mecahnisms*, 2019, no. 2013.

[19] T. Letcher and M. Waytashek, "Material Property Testing of 3D-Printed Specimen," *Proceedings of the ASME 2014 International Mechanical Engineering Congress and Exposition*, pp. 1–8, 2016.

[20] J. R. C. Dizon, A. H. Espera, Q. Chen, and R. C. Advincula, "Mechanical characterization of 3D-printed polymers," pp. 44–67, 3 2018.

[21] Y. Song, Y. Li, W. Song, K. Yee, K. Y. Lee, and V. L. Tagarielli, "Measurements of the mechanical response of unidirectional 3D-printed PLA," *Materials and Design*, vol. 123, pp. 154–164, 6 2017.

[22] "Tracker Video Analysis Tool." [Online]. Available: https://physlets.org/tracker/